Observer Design for Boundary Coupled PDEs

Application to Thermostatically Controlled Loads in Smart Grids

Moura, Scott; Bendtsen, Jan Dimon; Ruiz, Victor

Published in:
Decision and Control (CDC), 2013 IEEE 52nd Annual Conference on

DOI (link to publication from Publisher):
10.1109/CDC.2013.6760883

Publication date:
2013

Document Version
Accepted author manuscript, peer reviewed version

52nd IEEE Conference on Decision and Control
December 10-13, 2013. Florence, Italy

Observer Design for Boundary Coupled PDEs: Application to Thermostatically Controlled Loads in Smart Grids

Scott Moura, *Member, IEEE* Jan Bendtsen, *Member, IEEE* Victor Ruiz

***Abstract*— This paper develops methods for state estimation of aggregated thermostatically controlled loads (TCLs) in smart grids, via partial differential equation (PDE) techniques. TCLs include on/off controlled devices, such as heat pumps, HVAC systems, and deep freezers. Control of aggregated TCLs provides a promising opportunity to mitigate the mismatch between power generation and demand, thus enhancing grid reliability and enabling renewable energy penetration. However, persistent communication between thousands of TCLs to a central server can be prohibitive. To this end, this paper focuses on designing a state estimation scheme for a PDE-based model of aggregated TCLs, thus reducing the required communication. First, a two-state linear hyperbolic PDE model for homogenous TCL populations is presented. This model is extended to heterogeneous populations by including a diffusive term. Next, a state observer is derived, which uses only measurements of how many TCLs turn on/off at any given time. The design is proven to be exponentially stable via backstepping techniques. Finally, the observer's properties are demonstrated via simulation examples. The estimator provides system-critical information for power system monitoring and control.**

I. Introduction

One of the main challenges in achieving significant penetration of renewables in future power systems is their inherent variability. To this end, *demand side management* (DSM) has gained attention in recent years as a means to balance power supply and demand [1], in the presence of intermittent power sources. In particular, one may exploit the flexibility and large number of thermostatically controlled loads (TCLs) to enhance grid reliability and enable renewable energy penetration [2], [3]. However, to leverage the full potential of DSM schemes, one requires mathematical models that describe their dynamical behavior [3], [4], [5], [6], [7].

In this paper we examine estimation of the distribution of temperature in aggregated TCL populations. This information can be utilized to confidently manipulate the temperature set points to shape the aggregated TCL power consumption. That is, the population can be used as a fast "virtual power plant" which provides control services to the grid. This includes frequency control reserves and peak shaving, where energy in the form of displaced consumption can be traded on electricity spot markets. Precise information about the available storage reserves provides the system operator with greater flexibility for providing such services in a reliable manner while ensuring quality of service to consumers.

We consider a large population of TCLs and derive a partial differential equation (PDE)-based model of the temperature distribution evolution. Such PDE models of TCL populations were also studied in [6] and [8]. The latter papers, in particular, presented models that account for heterogeneity among the TCLs by including a diffusion term in the PDEs, along with various methods for parameter identification. Markov chain models are also used to account for parameter heterogeneity and design Kalman filtering state estimation schemes [9].

In this paper, we extend the aforementioned work by presenting an observer design for online monitoring of the PDE state (i.e. distribution of TCL temperature) using minimal sensing and communication. That is, individual TCLs only send data when switching between heating and cooling. Mathematically, these measurements manifest themselves as PDE boundary measurements. Consequently, the observer is designed via PDE backstepping methods [10], [11]. Mathematically, this paper develops a boundary observer for boundary-coupled parabolic equations, a unique contribution to the authors' knowledge.

The outline of this paper is as follows. In Section II we briefly recall the models on which we base the observer design. Section III presents the observer design and associated stability analysis. Finally, Section IV presents simulations and Section and V summarizes the contributions.

II. Modeling Aggregations of TCLs

We first consider the following hybrid ODE model of a single TCL. Let the internal and ambient temperatures of the i'th TCL affected by the action of the heating/cooling hardware be denoted T_i and $T_{\infty,i}$, respectively. Assume the hardware is purely on/off-regulated. The temperature dynamics are governed by

$$\dot{T}_i(t) = \frac{1}{R_i C_i}\left[T_{\infty,i} - T_i(t) - s_i(t) R_i P_i\right], \quad i = 1,2,\ldots,N, \quad (1)$$

$$s_i(t) = \begin{cases} 0 & \text{if } s_i(t-\varepsilon) = 1 \text{ and } T_i(t) \le T_{\min,i} \\ 1 & \text{if } s_i(t-\varepsilon) = 0 \text{ and } T_i(t) \ge T_{\max,i} \\ s_i(t-\varepsilon) & \text{otherwise} \end{cases} \quad (2)$$

for some small time ε. The symbol $C_i \in \mathbb{R}_+$ is the thermal capacitance (kWh/°C) of the consumer, $R_i \in \mathbb{R}_+$ is the corresponding thermal resistance (°C/kW) and $P_i \in \mathbb{R}$ is the (constant) heating/cooling power supplied by the hardware when switched on. Variable $s_i \in \{0,1\}$ is a Boolean-valued

S. Moura is with Civil and Environmental Engineering, University of California, Berkeley, CA 94720, USA smoura@berkeley.edu

J. Bendtsen is with the Department of Electronic Systems, Automation and Control, Aalborg University, 9210 Aalborg, Denmark dimon@es.aau.dk

V. Ruiz is with the Department of Mechanical and Aerospace Engineering, University of California, San Diego, La Jolla, CA 92093-0411, USA viruiz@ucsd.edu

978-1-4673-5716-6/13/$31.00 ©2013 IEEE

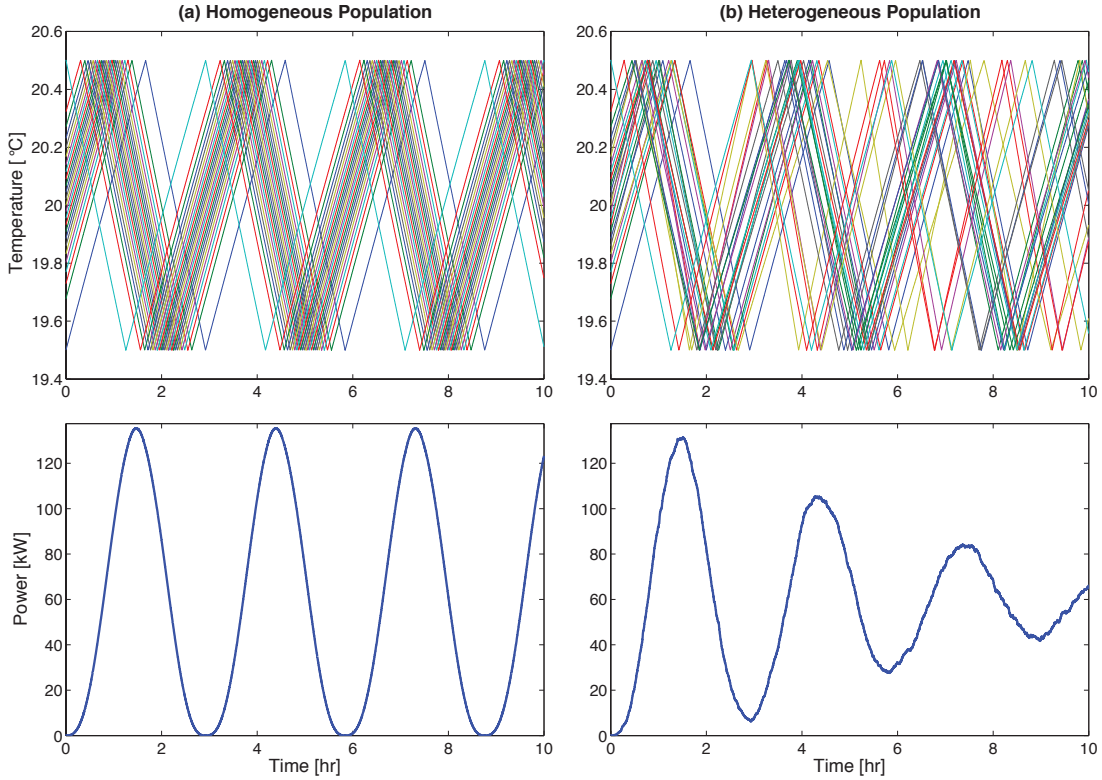

Fig. 1. Evolution of temperature for 25 TCLs from (a) homogeneous and (b) heterogeneous populations. In each case, the population was initialized with all TCLs in the *off* state, with temperatures quadratically distributed around 20°C. Note the TCLs remain in synchrony for the homogenous population. In contrast, the temperature distribution diffuses in the heterogeneous case. This observation motivates the heterogeneous model in Section II-B.

variable that switches status whenever the internal temperature encounters the limits of a pre-set temperature span $[T_{\min,i}, T_{\max,i}] \subset \mathbb{R}$, denoting the cooling or heating state.

The temperature limits $T_{\min,i}$ and $T_{\max,i}$ are related to the i'th TCL *setpoint* $T_{\text{sp},i}$ through the fixed relations,

$$T_{\min,i} = T_{\text{sp},i} - \frac{\Theta}{2}, \quad T_{\max,i} = T_{\text{sp},i} + \frac{\Theta}{2},$$

where Θ is the width of the temperature interval. Furthermore, the cumulative power consumption of the entire population at any given time t can be computed as

$$P(t) = \sum_i \frac{1}{\eta_i} P_i s_i(t) \tag{3}$$

where η_i is the coefficient of performance for the i'th heating/cooling unit. Assuming that it is possible to adjust the setpoint $T_{\text{sp},i}$ of a large number of TCLs, it becomes possible to intelligently shape the aggregated power consumption. Thus, $T_{\text{sp},i}$ is of interest for control purposes. However, since this paper's focus is on estimation, we will disregard controllable setpoints in this model.

A. Homogeneous population

Now consider a large population of the individual TCLs described above. Let the continuously differentiable functions $u(T,t)$ and $v(T,t)$, both defined on the spaces $[T_{\min}, T_{\max}] \times \mathbb{R}_+ \to \mathbb{R}_+$, denote the distribution of loads at temperature T and time t in the *on* and *off* states, respectively. By considering the 'flow' of TCLs along the temperature axis in either the positive or negative directions, and taking limits, it is possible to derive the following PDE model for a homogeneous population of TCLs [6], [8]:

$$u_t(T,t) = \alpha\lambda(T)u_T(T,t) + \alpha u(T,t), \tag{4}$$
$$v_t(T,t) = -\alpha\mu(T)v_T(T,t) + \alpha v(T,t), \tag{5}$$
$$u(T_{\max},t) = q_1 v(T_{\max},t), \tag{6}$$
$$v(T_{\min},t) = q_2 u(T_{\min},t), \tag{7}$$

where subscripts $(\cdot)_T$ and $(\cdot)_t$ indicate partial derivative of $(\cdot)$ w.r.t. temperature and time, respectively. The parameters $\alpha, \lambda(T), \mu(T), q_1, q_2$ are given by

$$\alpha = \frac{1}{\bar{R}\bar{C}} > 0, \tag{8}$$
$$\lambda(T) = -(T_\infty - T - \bar{R}\bar{P}) > 0, \quad \mu(T) = T_\infty - T > 0, \tag{9}$$
$$q_1 = -\frac{T_\infty - T_{\max}}{T_\infty - T_{\max} - \bar{R}\bar{P}}, \quad q_2 = -\frac{T_\infty - T_{\min} - \bar{R}\bar{P}}{T_\infty - T_{\min}}. \tag{10}$$

Since all the TCLs are assumed to be identical, $\bar{R}, \bar{P}$ and $\bar{C}$ are the population-wide values for R_i, P_i and C_i, respectively.

The power consumption of the entire population may be obtained by integrating the distribution of TCLs in the *on*-state:

$$P(t) = \frac{\overline{P}}{\eta} \int_{T_{min}}^{T_{\max}} u(T,t)dT, \tag{11}$$

where $\bar{P}$ is the (constant) power delivered to each TCL in the *on* state and η is the coefficient of performance.

Figure 1 demonstrates the aggregated behavior for 25 identical TCLs. The left plots show how the TCLs alternate between the *on* and *off* states while remaining within the operation band. The TCLs were initiated at random temperatures, quadratically distributed around 20°C, all in the *off* state. As can be seen, the power exhibits undamped oscillations, since the TCLs are synchronized.

The right plots in Fig. 1 show a similar situation, but instead of being identical, the time constants of TCLs have now been drawn from a random distribution, thus making the population *heterogenous*. Due to different time constants, and hence variations in the duty cycles, the individual TCLs gradually de-synchronize and the oscillations in power consumption damp out. Similar effects occur if other parameters, such as Θ_i or $T_{\infty,i}$, are allowed to vary across the TCL population.

B. Heterogeneous population

Next we consider a PDE model for *heterogenous* populations of TCLs. Motivated by the diffusive phenomenon observed in the Monte Carlo simulations of heterogeneous populations, we consider the following novel diffusion-advection model [8]:

$$u_t(T,t) = \alpha\lambda(T)u_T(T,t) + \alpha u(T,t) + \beta u_{TT}(T,t), \quad (12)$$
$$v_t(T,t) = -\alpha\mu(T)v_T(T,t) + \alpha v(T,t) + \beta v_{TT}(T,t), \quad (13)$$

$$u(T_{\max},t) = q_1 v(T_{\max},t), \quad (14)$$
$$v(T_{\min},t) = q_2 u(T_{\min},t), \quad (15)$$
$$u_T(T_{\min},t) = -v_T(T_{\min},t), \quad (16)$$
$$v_T(T_{\max},t) = -u_T(T_{\max},t). \quad (17)$$

This model adds diffusion terms to PDEs (4)-(5) to incorporate parameter heterogeneity. The two boundary conditions (16)-(17) are added to preserve well-posedness of the PDE system. Figure 2 illustrates the improved modeling capabilities of adding the diffusive term.

III. Observer Design

A. Low-bandwidth measurement feedback

Monitoring aggregations of TCLs, using the PDE models derived above, requires measurement feedback. If the TCLs are equipped with sophisticated measurement equipment, it is possible to measure the temperature online and continuously transmit data to a central server. However, if the TCL populations grow large, this strategy may place an intractably heavy load on the communication infrastructure [9]. Therefore, we propose a unique strategy that requires significantly less communication bandwidth, oriented toward boundary measurements of the PDE model (12)–(17); see Figure 3.

Figure 3 illustrates the temperature response of a single TCL. The local controller records the timing t_1' when the temperature crosses a pre-set value slightly smaller than $T_{\max}$. Then the TCL's power switches on at time t_1, when

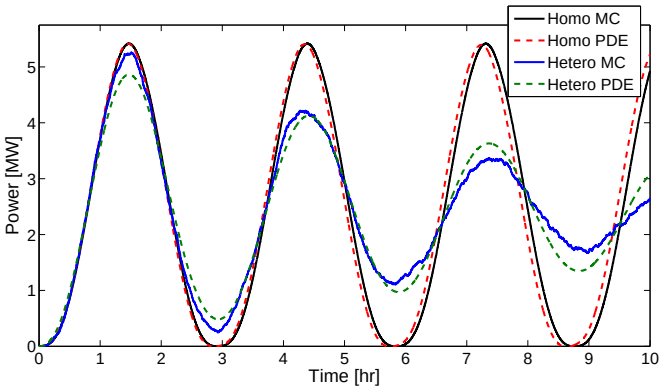

Fig. 2. Comparison of aggregate TCL power for the homogeneous and heterogeneous populations, using the 1,000 individual TCLs in the Monte Carlo (MC) model and the PDE models. The heterogeneous PDE model captures the damped oscillations exhibited by the heterogeneous MC model.

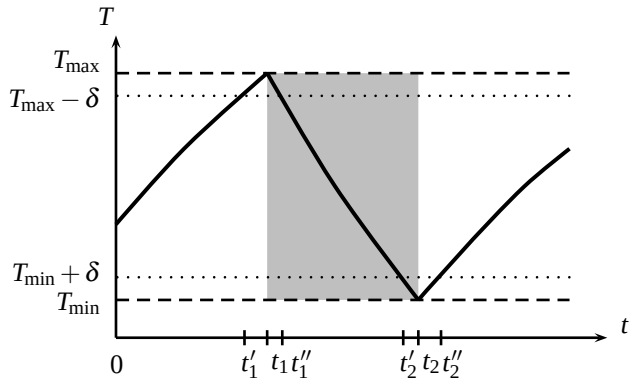

Fig. 3. Illustration of TCL measurement feedback. The TCL records the temperature just before (t_i'), at (t_i) and just after (t_i'') the temperature reaches $T_{\max}$. A similar process is performed around $T_{\min}$. The gray area indicates that cooling power is turned on.

the temperature reaches $T_{\max}$. Finally, the local controller records the timing t_1'' when the temperature drops below $T_{\max}-\delta$. A similar procedure is carried out when the temperature reaches $T_{\min}+\delta$. These measurements are submitted as they occur to the central server, allowing estimation of $u(T_{\min}), v(T_{\max})$, *as well as* the corresponding spatial derivatives $u_T(T_{\max}), v_T(T_{\min})$ based on t_i' and t_i''.

B. Preliminaries

First we normalize the spatial coordinate to simplify our analysis

$$x = \frac{T - T_{\min}}{T_{\max} - T_{\min}}, \quad (18)$$

which renders the heterogenous PDE into,

$$u_t(x,t) = \alpha\breve{\lambda}(x)u_x(x,t) + \alpha u(x,t) + \breve{\beta}u_{xx}(x,t), \quad (19)$$
$$v_t(x,t) = -\alpha\breve{\mu}(x)v_x(x,t) + \alpha v(x,t) + \breve{\beta}v_{xx}(x,t), \quad (20)$$
$$u(1,t) = q_1 v(1,t), \qquad u_x(0,t) = -v_x(0,t), \quad (21)$$
$$v(0,t) = q_2 u(0,t), \qquad v_x(1,t) = -u_x(1,t), \quad (22)$$

where the parameters $\breve{\lambda}(x), \breve{\mu}(x), \breve{\beta}$ are given by

$$\breve{\lambda}(x) = x - \frac{T_\infty - T_{\min} - RP}{T_{\max} - T_{\min}}, \quad (23)$$

$$\breve{\mu}(x) = \frac{T_\infty - T_{\min}}{T_{\max} - T_{\min}} - x, \quad (24)$$

$$\breve{\beta} = \frac{\beta}{(T_{\max} - T_{\min})^2}. \quad (25)$$

To reduce notational clutter, the breves are henceforth dropped from $\breve{\lambda}(x), \breve{\mu}(x), \breve{\beta}$. Additionally, we drop the arguments of the states, when they are clear from context.

C. Observer Design

In the following observer design, we assume availability of $u(0), v(1), u_x(1), v_x(0)$ for measurement, as described in Section III-A. Consider the following observer design,

$$\begin{aligned}
\hat{u}_t(x,t) &= \alpha\lambda(x)\hat{u}_x(x,t) + \alpha\hat{u}(x,t) + \beta\hat{u}_{xx}(x,t) \\
&\quad + p_1(x)\left[u(0,t) - \hat{u}(0,t)\right], && (26)\\
\hat{u}_x(0,t) &= -v_x(0,t) + p_{10}\left[u(0,t) - \hat{u}(0,t)\right], && (27)\\
\hat{u}(1,t) &= q_1 v(1,t), && (28)\\
\hat{v}_t(x,t) &= -\alpha\mu(x)\hat{v}_x(x,t) + \alpha\hat{v}(x,t) + \beta\hat{v}_{xx}(x,t) \\
&\quad + p_2(x)\left[v(1,t) - \hat{v}(1,t)\right], && (29)\\
\hat{v}(0,t) &= q_2 u(0,t), && (30)\\
\hat{v}_x(1,t) &= -u_x(1,t) + p_{20}\left[v(1,t) - \hat{v}(1,t)\right]. && (31)
\end{aligned}$$

This renders the following dynamics for the error system $\tilde{u} = u - \hat{u}$,

$$\begin{aligned}
\tilde{u}_t &= \alpha\lambda(x)\tilde{u}_x + \alpha\tilde{u} + \beta\tilde{u}_{xx} - p_1(x)\tilde{u}(0), && (32)\\
\tilde{u}_x(0) &= -p_{10}\tilde{u}(0), && (33)\\
\tilde{u}(1) &= 0, && (34)
\end{aligned}$$

and error system $\tilde{v} = v - \hat{v}$,

$$\begin{aligned}
\tilde{v}_t &= -\alpha\mu(x)\tilde{v}_x + \alpha\tilde{v} + \beta\tilde{v}_{xx} - p_2(x)\tilde{v}(1), && (35)\\
\tilde{v}_x(0) &= 0, && (36)\\
\tilde{v}_x(1) &= -p_{20}\tilde{v}(1). && (37)
\end{aligned}$$

Note that the error systems are decoupled. Consequently, we may design the observer gains for each system separately.

Before proceeding with the observer design, we apply the following invertible "gauge" transformations to eliminate the advection terms,

$$\xi(x,t) = \tilde{u}(x,t)e^{\frac{\alpha}{2\beta}\int_0^x \lambda(s)ds}, \quad (38)$$

$$\eta(x,t) = \tilde{v}(x,t)e^{\frac{\alpha}{2\beta}\int_x^1 \mu(s)ds}. \quad (39)$$

The transformed states ξ and η satisfy the following reaction-diffusion PDEs,

$$\begin{aligned}
\xi_t &= \beta\xi_{xx} + g(x)\xi(x,t) - p_1^\xi(x)\xi(0), && (40)\\
\xi(0) &= p_{10}^\xi \xi(0), && (41)\\
\xi(1) &= 0, && (42)
\end{aligned}$$

$$\begin{aligned}
\eta_t &= \beta\eta_{xx} + h(x)\eta(x,t) - p_2^\eta(x)\eta(1), && (43)\\
\eta(0) &= 0, && (44)\\
\eta_x(1) &= p_{20}^\eta \eta(1), && (45)
\end{aligned}$$

where

$$\begin{aligned}
g(x) &= \alpha\left[1 - \frac{\lambda'(x)}{2}\right] - \frac{\alpha^2\lambda^2(x)}{4\beta}, && (46)\\
p_1^\xi(x) &= p_1(x)e^{\frac{\alpha}{2\beta}\int_0^x \lambda(s)ds}, && (47)\\
p_{10}^\xi &= \frac{\alpha}{2\beta}\lambda(0) - p_{10}, && (48)
\end{aligned}$$

$$\begin{aligned}
h(x) &= \alpha\left[1 + \frac{\mu'(x)}{2}\right] - \frac{\alpha^2\mu^2(x)}{4\beta}, && (49)\\
p_2^\eta(x) &= p_2(x)e^{\frac{\alpha}{2\beta}\int_x^1 \mu(s)ds}, && (50)\\
p_{20}^\eta &= -\frac{\alpha}{2\beta}\mu(1) - p_{20}. && (51)
\end{aligned}$$

Remark 1 Note that this transformation does not assume the advection dynamics are negligible. Instead, it absorbs the advection terms into the reaction terms and boundary conditions. This will simplify our observer design, and renders the error dynamics into a form which leverages existing results [10]. ◁

1) Backstepping Transformation: Next we apply the PDE backstepping approach [10]. That is, we consider the following transformations for the error system states

$$\xi(x,t) = w_1(x,t) - \int_0^x p(x,y)w_1(y,t)dy, \quad (52)$$

$$\eta(x,t) = w_2(x,t) - \int_x^1 q(x,y)w_2(y,t)dy, \quad (53)$$

where $w_1(x,t)$ and $w_2(x,t)$ are the states for the target systems, described next.

2) Target System: We seek transformations (52)-(53) which transform the error systems (40)–(45) into the exponentially stable (for $c_1, c_2 \geq 0$) target systems,

$$\begin{aligned}
w_{1t}(x,t) &= \beta w_{1xx}(x,t) - c_1 w_1(x,t), && (54)\\
w_{1x}(0,t) &= w_1(0,t), && (55)\\
w_1(1,t) &= 0, && (56)\\
w_{2t}(x,t) &= \beta w_{2xx}(x,t) - c_2 w_2(x,t), && (57)\\
w_2(0,t) &= 0, && (58)\\
w_{2x}(1,t) &= -w_2(1,t). && (59)
\end{aligned}$$

The parameters c_1 and c_2 can be adjusted to tune the observers' convergence speed. To characterize convergence speed, consider the spatial L_2 norms as Lyapunov functions, that is $V_1 = \int_0^1 w_1^2(x,t)dx$ and $V_2 = \int_0^1 w_2^2(x,t)dx$. One can show that the derivatives of V_1 and V_2 along the solution trajectories are upper bounded by

$$\dot{V}_1 \leq -\left[\frac{1}{2}\beta + 2c_1\right]V_1, \quad (60)$$

$$\dot{V}_2 \leq -\left[\frac{1}{2}\beta + 2c_2\right]V_2. \quad (61)$$

Using the comparison principle, we obtain an upper bound on the evolution of the states' L_2 norms

$$\|w_1(x,t)\|_{L_2} \leq \|w_1(x,0)\|_{L_2} e^{-\left[\frac{1}{2}\beta+2c_1\right]t}, \quad (62)$$

$$\|w_2(x,t)\|_{L_2} \leq \|w_2(x,0)\|_{L_2} e^{-\left[\frac{1}{2}\beta+2c_2\right]t}, \quad (63)$$

where the convergence speeds increase as c_1 and c_2 increase.

3) Kernel PDE: Next, we determine the kernel functions $p(x,y)$ and $q(x,y)$ in (52) and (53), which transform the error dynamics into the target systems. After substituting (52) into (40)-(42), we obtain a set of conditions for $p(x,y)$,

$$\beta p_{xx}(x,y) - \beta p_{yy}(x,y) = -[c_1 + g(x)]\, p(x,y), \quad (64)$$

$$p(x,x) = -\frac{1}{2\beta}\int_x^1 [c_1 + g(s)]\, ds, \quad (65)$$

$$p(1,y) = 0. \quad (66)$$

These conditions constitute a hyperbolic PDE, defined over the triangular domain $\mathscr{D}_1 = \{(x,y)|0 < y < x < 1\}$. The observer gains are given by the solution of $p(x,y)$ as follows,

$$p_1^{\xi}(x) = -\beta\,[p(x,0) + p_y(x,0)], \quad (67)$$

$$p_{10}^{\xi} = 1 - p(0,0). \quad (68)$$

Similarly, we substitute (53) into (43)-(45) to obtain a PDE for kernel $q(x,y)$,

$$\beta q_{xx}(x,y) - \beta q_{yy}(x,y) = -[c_2 + h(x)]\, q(x,y), \quad (69)$$

$$q(x,x) = -\frac{1}{2\beta}\int_0^x [c_2 + h(s)]\, ds, \quad (70)$$

$$q(0,y) = 0, \quad (71)$$

defined over the triangular domain $\mathscr{D}_2 = \{(x,y)|0 < x < y < 1\}$. The observer gains for the η subsystem are given by

$$p_2^{\eta}(x) = -\beta\,[q(x,1) + q_y(x,1)], \quad (72)$$

$$p_{20}^{\eta} = q(1,1) - 1. \quad (73)$$

D. Main Results

The following lemma states that the kernel PDEs (64)-(66) and (69)-(71) are solvable. Moreover, it states that the transformations (52)-(53) are invertible, which means that stability of the target systems implies stability of the (ξ,η) system, and consequently the original $(\tilde{u},\tilde{v})$ system.

Lemma 1 (Well Posedness and Invertability [10]): The kernel PDEs (64)-(66) and (69)-(71) have unique $C^2(\mathscr{D}_1)$ and $C^2(\mathscr{D}_2)$ solutions, $p(x,y)$ and $q(x,y)$, respectively. The kernels $r_1(x,y)$ and $r_2(x,y)$ of the inverse transformations

$$w_1(x,t) = \xi_1(x,t) + \int_0^x r_1(x,y)\xi(y,t)dy, \quad (74)$$

$$w_2(x,t) = \eta(x,t) + \int_x^1 r_2(x,y)\eta(y,t)dy, \quad (75)$$

also have unique $C^2(\mathscr{D}_1)$ and $C^2(\mathscr{D}_2)$ solutions, respectively.

Proof: It has been shown in [10] that PDEs (64)-(66) and (69)-(71) are well posed. Equations (64)-(66) match a special case of (16)-(18) in [10]. Equations (69)-(71) match a special case of (39)-(41) in [10] as well. Therefore, well posedness of these PDEs and invertability of transformations (52) and (53) follow immediately. ■

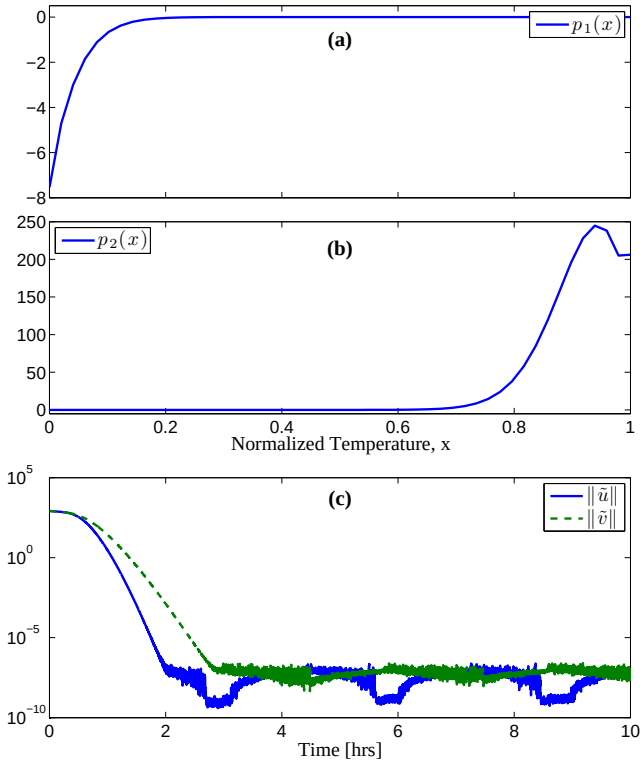

Fig. 4. The output injection gains $p_1(x)$ and $p_2(x)$ are provided in (a) and (b), respectively. Subplot (c) demonstrates how the L_2 norms of the estimation error, $\|\tilde{u}\|, \|\tilde{v}\|$, decay toward zero.

We are now positioned to state our main result on exponential stability of the estimation error system.

Theorem 1 (Exponential stability): Let $p(x,y)$ and $q(x,y)$ be the respective solutions of kernel PDEs (64)-(66) and (69)-(71). Consider any initial condition $\tilde{u}_0(x), \tilde{v}_0(x) \in L_2(0,1)$. Also consider output injection gains $p_1(x), p_{10}, p_2(x), p_{20}$ given by (47), (48), (50) (51), (67), (68), (72) (73). Under these conditions, $\tilde{u}(x,t), \tilde{v}(x,t)$ have unique $C^{2,1}((0,1)\times(0,\infty))$ solutions. Additionally, the origins $\tilde{u}(x,t) = \tilde{v}(x,t) = 0$ are exponentially stable in the $L_2(0,1)$ norm, as characterized by (62)-(63), for tunable parameters $c_1, c_2 \geq 0$.

IV. Simulation Example

Next we examine the observer's performance via simulations. In these simulations, we select target system parameters $c_1 = c_2 = 10$. The TCL model parameters are $R = 2°\text{C/kW}$, $C = 10$ kWh/°C, $P = 14$kW, $T_\infty = 32°\text{C}$, $T_{sp} = 20°\text{C}$, $\Theta = 1°\text{C}$, $\eta = 2.5$, $\beta = 0.0145$ [3], [5]. For the purpose of demonstrating the results, model data is generated from the heterogeneous PDE (12)-(17). The observer is initialized with an incorrect state, namely $\hat{u}(T,t_0) = v(T,t_0)$ and $\hat{v}(T,t_0) = u(T,t_0)$. To solve the kernel PDEs (64)-(66) and (69)-(71), we convert these equations to integral equations and use the method of successive approximations [11]. The resulting solutions for the output error injection gains $p_1(x)$

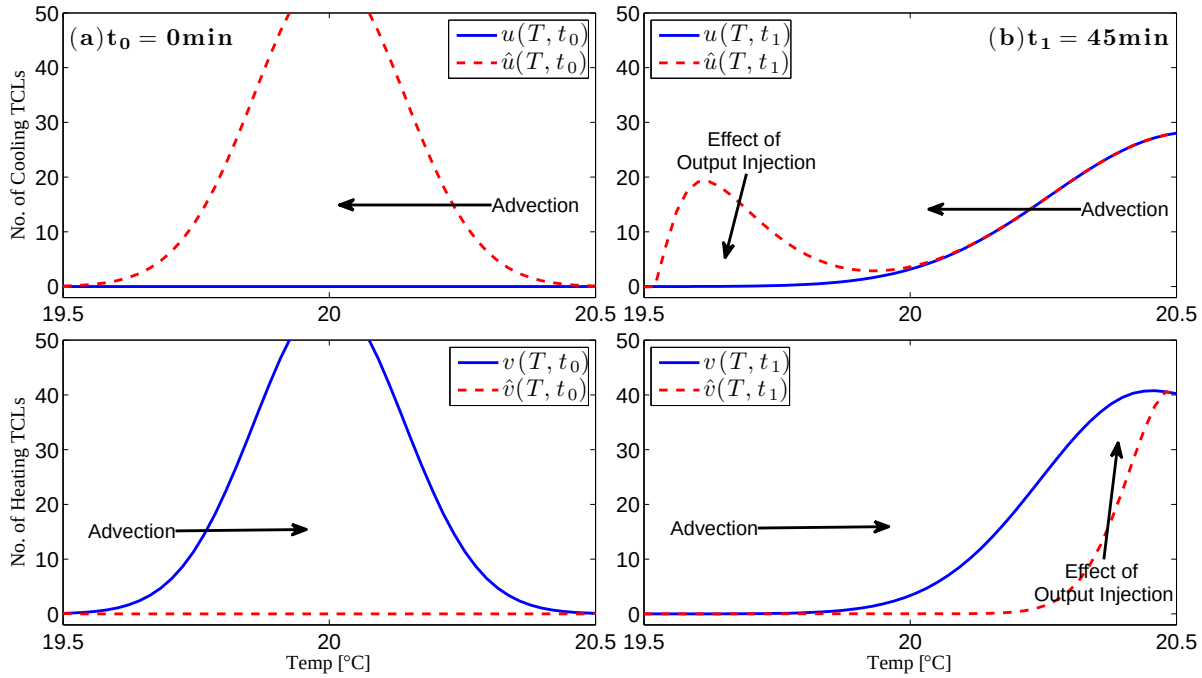

Fig. 5. The left side (a) and right side (b) depict snapshots of the true and estimated states, at times $t_0 = 0$ min and $t_1 = 45$ min, respectively. In (a), the observer is initialized with an incorrect state, namely $\hat{u}(T,t_0) = v(T,t_0)$ and $\hat{v}(T,t_0) = u(T,t_0)$. Subplot (b) depicts how the output error injection corrects the "outlet" end of the flow, whereas the system's natural advection corrects the "inlet" end.

and $p_2(x)$ are depicted in Fig. 4(a) and (b), respectively. The scalar gains are $p_{10} = 55.17$ and $p_{20} = 115.83$.

Figure 4(c) demonstrates how the L_2 norms of the estimation error, $\|\tilde{u}\|, \|\tilde{v}\|$, decay toward zero. Figure 5 displays two snapshots of the true and estimated states, at times $t_0 = 0$ min and $t_1 = 45$ min. These plots exemplify how the observer corrects the model dynamics. Note that $p_1(x)$ and $p_2(x)$ have greater magnitude at the "outlet" end of the temperature domain. The interpretation is the observer corrects the "outlet" end of the flow, whereas the system's natural advection corrects the "inlet" end. Consequently, the aggregated TCL observer converges to the true temperature distribution by intelligently combining (low-bandwidth) measurements and the population's natural dynamical properties.

V. Conclusions

This paper examines modeling and state estimation of aggregated TCL populations, for monitoring in demand-side management programs, e.g. frequency control reserves, peak shaving. We present two PDE models of aggregated TCLs, for both homogenous and heterogeneous populations. The main contribution is the derivation of an observer for online monitoring of the PDE 'state' (distribution of TCL temperature). The design uses only boundary measurements in the form of data transmitted when a TCL switches between heating and cooling, thus keeping communication requirements low. The observer is constructed using PDE backstepping methods. Simulation studies demonstrate the observer's convergence properties, and provide intuition for its behavior. Further studies investigate model uncertainty, measurement noise, and performance on real-world data.

References

[1] G. Strbac, "Demand side management: Benefits and challenges," *Energy Policy*, vol. 36, no. 12, pp. 4419–4426, 2008.

[2] R. Malhame and C. Chong, "Electric load model synthesis by diffusion approximation of a higher-order hybrid-state stochastic system," *IEEE Transactions on Automatic Control*, vol. 30, no. 9, pp. 854–860, 1985.

[3] D. Callaway, "Tapping the energy storage potential in electric loads to deliver load following and regulation, with application to wind energy," *Energy Conversion and Management*, vol. 50, no. 9, pp. 1389–1400, 2009.

[4] S. Kundu and N. Sinitsyn, "Safe protocol for controlling power consumption by a heterogeneous population of loads," in *Proc. of 2012 American Control Conference*, June 2012.

[5] C. Perfumo, E. Kofman, J. Braslavsky, and J. Ward, "Load management: Model-based control of aggregate power for populations of thermostatically controlled loads," *Energy Conversion and Management*, vol. 55, no. 1, pp. 36–48, 2012.

[6] S. Bashash and H. Fathy, "Modeling and control of aggregate air conditioning loads for robust renewable power management," *IEEE Transactions on Control Systems Technology*, vol. 21, no. 4, pp. 1318–1327, 2013.

[7] W. Zhang, J. Lian, C.-Y. Chang, K. Kalsi, and Y. Sun, "Reduced-order modeling of aggregated thermostatic loads with demand response," in *Proc. of 51st IEEE Conference on Decision and Control*, Dec. 2012.

[8] S. Moura, J. Bendtsen, and V. Ruiz, "Modeling Heterogeneous Populations of Thermostatically Controlled Loads Using Diffusion-Advection PDEs," in *Proceedings of the 2013 ASME Dynamic Systems and Control Conference*, Stanford, California, Oct. 2013.

[9] J. L. Mathieu, S. Koch, and D. S. Callaway, "State estimation and control of electric loads to manage real-time energy imbalance," *IEEE Transactions on Power Systems*, vol. 28, no. 1, pp. 430 –440, Feb. 2013.

[10] A. Smyshlyaev and M. Krstic, "Backstepping observers for a class of parabolic PDEs," *Systems & Control Letters*, vol. 54, no. 7, pp. 613–625, 2005.

[11] M. Krstic and A. Smyshlyaev, *Boundary Control of PDEs: A Course on Backstepping Designs*. Philadelphia, PA: Society for Industrial and Applied Mathematics, 2008.